Approximation of boundary element matrices using GPGPUs and nested cross approximation

Steffen Börm[a,*], Sven Christophersen[a]

[a]*Department of Computer Science, Christian-Albrechts-Universität zu Kiel, 24118 Kiel, Germany*

arXiv:1510.07244v2 [cs.MS] 18 Oct 2017

Abstract

The efficiency of boundary element methods using a Galerkin discretization depends crucially on the time required for setting up the stiffness matrix. The far-field part of the matrix can be approximated by compression schemes like the fast multipole method or $\mathcal{H}$-matrix techniques. The near-field part is typically approximated by special quadrature rules like the Sauter-Schwab technique that can handle the singular integrals appearing in the diagonal and near-diagonal matrix elements.

Since computing one element of the matrix requires only a small amount of data but a fairly large number of operations, we propose to use general-purpose graphics processing units (GPGPUs) to handle vectorizable portions of the computation: near-field computations are ideally suited for vectorization and can therefore be handled very well by GPGPUs. Modern far-field compression schemes can be split into a small adaptive portion that exhibits divergent control flows, and should therefore be handled by the CPU, and a vectorizable portion that can again be sent to GPGPUs.

We propose a hybrid algorithm that splits the computation into tasks for CPUs and GPGPUs. The method presented in this article is able to reduce the setup time of boundary integral operators by a significant factor of 19–30 for both the Laplace and the Helmholtz equation in 3D when using two consumer GPGPUs compared to a quad-core CPU.

Keywords: Boundary element method, GPGPU, hierarchical matrix

1. Introduction

Compared to the popular finite element methods, boundary element methods offer advantages like improved accuracy and the possibility to handle infinite domains, but these advantages come at the price of a stiffness matrix that is no longer sparse and requires us to evaluate singular integrals.

During the last decades, both issues have been the focus of significant research activities: approximation schemes like the fast multipole method [26, 15, 1, 13, 33, 25], panel clustering [20, 28], or hierarchical matrices [17, 18, 2, 14, 7] replace the stiffness matrix by a data-sparse approximation of arbitrary accuracy that can be computed in almost linear complexity. State-of-the-art compression schemes relying on $\mathcal{H}^2$-matrices [19, 8, 4, 3, 5] can handle matrices with millions of degrees of freedom in minutes on modern computers.

Graphics processors, originally developed to speed up CAD applications and computer games, have in the past years been generalized to handle far more general tasks. *General-purpose graphics processing units* (GPGPUs) offer computational resources far outstripping any CPU, e.g., thousands of arithmetic-logical units combined with high-bandwidth storage, but at the price of severe restrictions, e.g., only a limited amount of directly accessible memory and high sensitivity to divergent control flows inherited from their vector-oriented architecture.

Due to the computational power of GPGPUs, there have been attempts to utilize the computational power of GPGPUs to reduce setup times for discretized boundary integral operators [32, 24, 21, 31].

Modern compression techniques, e.g., hierarchical matrices ($\mathcal{H}$-matrices) or $\mathcal{H}^2$-matrices rely on adaptivity to obtain close to optimal compression rates. An example is the adaptive cross approximation (ACA) method [2, 3] that combines a heuristic pivoting strategy with a rank-revealing LR factorization.

Unfortunately, adaptive algorithms are generally not well-suited for GPGPUs: graphics processors are typically designed using a *single instruction, multiple data* (SIMD) architecture, i.e., groups of processing elements have to execute *the exact same instruction* in each clock cycle. Modern GPGPUs extend this to a *single instruction, multiple threads* (SIMT) approach that essentially allows some of the processing elements in a group to do nothing while the others execute one instruction. Adaptive algorithms typically iterate until a certain accuracy has been reached, i.e., the number of iterations depends on the input data. In an SIMD/SIMT architecture, this means that the run-time is determined by the slowest member of a group.

In order to avoid this problem, we propose a hybrid approach: adaptive parts of the algorithm are performed by CPUs, while non-adaptive parts like geometry transformations and numerical integration (quadrature) are handled by GPGPUs. The recently developed GCA compression scheme based on Green's

*Corresponding author.

Email addresses: boerm@email.uni-kiel.de (Steffen Börm), svc@informatik.uni-kiel.de (Sven Christophersen)

[1]Part of this work was funded by the Deutsche Forschungsgemeinschaft in the context of project BO 3289/2-1.

representation formula, quadrature, and nested cross approximation [6, 5] allows us to significantly reduce the adaptive parts of the algorithm and to take full advanage of the GPGPUs.

GCA can be split into an adaptive preparation phase that chooses suitable pivot elements for clusters and computes a number of small matrices, and a non-adaptive setup phase that computes matrix entries for the chosen pivot elements by quadrature.

We use the popular Sauter-Schwab quadrature technique [30, 27, 12, 29], since it relies mostly on arithmetic operations (addition, subtraction, multiplication, reciprocal square root) that modern GPGPUs can handle very efficiently. Another advantage of this quadrature technique is that each integral only requires a small amount of data, essentially only the coordinates of the vertices of two triangles, so there is a good chance that the memory bandwidth will not limit the performance of the central quadrature loop.

The Sauter-Schwab method distinguishes four cases: two triangles can be identical, they can share a common edge or a common vertex, or they can be completely disjoint. For each of these four cases, a number of quadrature points and weights are defined, with the "highly singular" first two cases requiring significantly more points than the last two cases. Heterogeneous systems are a good match for these rules: the main processor classifies the integrals according to the four categories and sorts them into work packages for the GPGPUs. Since all elements of a work package correspond to *exactly* the same quadrature rule, they are ideally suited for vector processors, and get sent to GPGPUs. Once all integrals in a work package have been handled, the results are returned to the main processor to be added to the final stiffness matrix. Even with comparably inexpensive mainstream GPGPUs, this approach can drastically reduce the runtime for singular and near-singular integrals.

2. Sequential algorithms

We consider the construction of an $\mathcal{H}^2$-matrix approximation of the stiffness matrix of a Galerkin BEM discretization.

2.1. Galerkin discretization

Given finite element bases $(\varphi_i)_{i\in\mathcal{I}}$ and $(\psi_j)_{j\in\mathcal{J}}$ for the test and trial spaces, a kernel function $g : \mathbb{R}^d \times \mathbb{R}^d \to \mathbb{C}$, and a submanifold $\Omega \subseteq \mathbb{R}^d$, the entries of the stiffness matrix $G \in \mathbb{C}^{\mathcal{I}\times\mathcal{J}}$ are given by

$$g_{ij} = \int_\Omega \varphi_i(x) \int_\Omega g(x,y)\psi_j(y)\,dy\,dx \tag{1}$$

for all $i \in \mathcal{I}$ and $j \in \mathcal{J}$. In this article, we focus on the kernel functions

$$g(x,y) = \frac{1}{4\pi\|x-y\|}, \qquad g(x,y) = \frac{\exp(\iota\kappa\|x-y\|)}{4\pi\|x-y\|} \tag{2}$$

corresponding to the Laplace and the Helmholtz equation. Here $\iota \in \mathbb{C}$ denotes the complex unit and $\kappa \in \mathbb{R}$ is the wave number.

Following the standard paradigm of finite element methods, the set Ω is represented by a grid $\mathcal{G}$ consisting of triangles $\Delta \in \mathcal{G}$. Representing the entries of G by

$$g_{ij} = \sum_{\Delta_\varphi\in\mathcal{G}} \sum_{\Delta_\psi\in\mathcal{G}} \int_{\Delta_\varphi} \varphi_i(x) \int_{\Delta_\psi} g(x,y)\psi_j(y)\,dy\,dx$$

for all $i \in \mathcal{I}$ and $j \in \mathcal{J}$, the task of computing these entries reduces to the task of evaluating integrals on the few pairs $(\Delta_\varphi, \Delta_\psi) \in \mathcal{G}\times\mathcal{G}$ of triangles where both basis functions φ_i and ψ_j do not vanish.

2.2. Sauter-Schwab quadrature

Assume that $\Delta_\varphi, \Delta_\psi \in \mathcal{G}$ are given. In order to evaluate the integral

$$\int_{\Delta_\varphi} \int_{\Delta_\psi} \varphi_i(x) g(x,y) \psi_j(y)\,dy\,dx,$$

we introduce the reference triangle

$$\widehat{\Delta} := \{(s,t) \in \mathbb{R}^2 \;:\; 0 \le t \le s \le 1\}$$

and affine maps $\Phi_\varphi : \widehat{\Delta} \to \Delta_\varphi$ and $\Phi_\psi : \widehat{\Delta} \to \Delta_\psi$. By the definition of surface integrals, we only have to evaluate

$$\sqrt{g_\varphi g_\psi} \int_{\widehat{\Delta}} \int_{\widehat{\Delta}} \varphi_i(\Phi_\varphi(\hat{x})) g(\Phi_\varphi(\hat{x}), \Phi_\psi(\hat{y})) \psi_j(\Phi_\psi(\hat{y}))\,d\hat{y}\,d\hat{x},$$

where the Gramian determinants are denoted by

$$g_\varphi := \det(D\Phi_\varphi^T D\Phi_\varphi), \qquad g_\psi := \det(D\Phi_\psi^T D\Phi_\psi).$$

For a polyhedral surface triangulation, both determinants are constant and can be computed in advance. Rewriting the integral with the transformed functions

$$\hat{\varphi}_i := \varphi_i \circ \Phi_\varphi, \quad \hat{\psi}_j := \psi_j \circ \Phi_\psi, \quad \hat{g}(\hat{x},\hat{y}) := g(\Phi_\varphi(\hat{x}), \Phi_\psi(\hat{y}))$$

yields

$$\int_{\widehat{\Delta}} \int_{\widehat{\Delta}} \hat{\varphi}_i(\hat{x}) \hat{g}(\hat{x},\hat{y}) \hat{\psi}_j(\hat{y})\,d\hat{y}\,d\hat{x}. \tag{3}$$

For standard finite element discretizations, the transformed basis functions $\hat{\varphi}_i$ and $\hat{\psi}_j$ are low-order polynomials that can be integrated easily. The transformed kernel function $\hat{g}$, on the other hand, poses a challenge: since typical kernel functions like the ones given in (2) have singularities at $x = y$, we have to evaluate singular integrals. The Sauter-Schwab quadrature rule [27, 29] uses transformations to remove these singularities, and the transformations depend on whether the triangles Δ_φ and Δ_ψ are identical, share a common edge, a common vertex, or are disjoint. In the last case, the integrand is smooth and we can apply standard quadrature. In the first three cases, the integrand has a singularity on a two-, one-, or zero-dimensional sub-manifold of the domain $\widehat{\Delta}\times\widehat{\Delta}$ of integration.

If Δ_φ and Δ_ψ are disjoint, there is no singularity, and we use the Duffy transformation

$$T : [0,1]^2 \to \widehat{\Delta}, \qquad (s,t) \mapsto (s, st),$$

to write (3) in the form

$$\int_{[0,1]^4} \xi_1\xi_3\, \hat{\varphi}_i(\xi_1, \xi_1\xi_2)\, \hat{g}(\xi_1, \xi_1\xi_2, \xi_3, \xi_3\xi_4)\, \hat{\psi}_j(\xi_3, \xi_3\xi_4)\, d\xi.$$

This integral can be approximated using standard tensor Gaussian quadrature.

For the singular cases, [29, §5.2] describes how the domain $\widehat{\Delta} \times \widehat{\Delta}$ can be split and transformed to obtain similar equations. Since each of the cases requires us to split the domain into a different number of subdomains, and since the transformations introduce additional polynomial factors, the number of quadrature points depends on the case, but not on anything else.

We can already see that Sauter-Schwab quadrature is particularly attractive for GPGPUs: the algorithm requires only the coordinates of the vertices of Δ_φ and Δ_ψ and then performs a relatively large number of operations, the evaluation of the kernel function and the basis functions in all quadrature points, so we have a fairly compute-intensive task. It is also clear that for each of the four cases exactly the same operations are carried out, only for different vertex data. This means that the work required to handle large number of pairs of triangles with the same type of singularity is ideally suited for vectorization.

Our algorithm considers pairs of triangles, determines the corresponding type of singularity, and creates work packages consisting of triangle pairs with the same type. Once the packages reach a given size, they are passed to the GPGPU that performs the quadrature and returns the results to the CPU that adds them to the appropriate coefficients in the matrix.

2.3. Green cross approximation

Computing all the entries of the matrix G would lead to an algorithm of quadratic complexity, and applying this algorithm to complicated geometries with a large number of triangles would involve a prohibitive computational cost.

This problem can be solved by replacing G by a *data-sparse approximations*, e.g., constructed by the fast multipole [26, 15, 16] or the panel-clustering [20] method. Since we already have an algorithm for computing entries of G at our disposal, we are looking for an approximation scheme that makes use of these entries. A well-known approach is the *adaptive cross approximation* (ACA) [2] that uses a rank-revealing LR factorization to construct blockwise low-rank approximations. This procedure is adaptive, i.e., the number of iterations of its main loop depends on the data that has to be approximated, so it is not particularly well-suited for GPGPUs.

The recently developed *Green-quadrature cross approximation* (GCA) algorithm [6, 5], on the other hand, can be split into a computationally inexpensive adaptive part and a far more expensive non-adaptive part. We can afford to treat the adaptive part on the CPU, while GPGPUs can take care of the bulk of the computation.

In order to derive the GCA method, we start with Green's representation formula

$$u(x) = \int_{\partial\omega} g(x,z) \frac{\partial u}{\partial n}(z)\, dz - \int_{\partial\omega} \frac{\partial g}{\partial n(z)}(x,z) u(z)\, dy$$

for harmonic functions u in a subdomain $\omega \subseteq \mathbb{R}^3$. If we pick $y \in \mathbb{R}^3 \setminus \bar{\omega}$, the restricted kernel function $x \mapsto g(x,y)$ is itself harmonic, and applying Green's formula yields

$$g(x,y) = \int_{\partial\omega} g(x,z) \frac{\partial g}{\partial n(z)}(z,y)\, dz - \int_{\partial\omega} \frac{\partial g}{\partial n(z)}(x,z) g(z,y)\, dz.$$

If we make sure that x and y are sufficiently far from the boundary $\partial\omega$ of the subdomain, both integrands appearing in this equation are smooth and can be approximated by standard quadrature rules, e.g., by a Gauß formula. This allows us to replace the integrals by weighted sums

$$g(x,y) \approx \sum_{\nu=1}^{m} w_\nu g(x,z_\nu) \frac{\partial g}{\partial n(z_\nu)}(z_\nu, y) \tag{4a}$$

$$- \sum_{\nu=1}^{m} w_\nu \frac{\partial g}{\partial n(z_\nu)}(x,z_\nu) g(z_\nu, y), \tag{4b}$$

where $(w_\nu)_{\nu=1}^m$ denotes the quadrature weights and $(z_\nu)_{\nu=1}^m$ denotes the quadrature points on the boundary $\partial\omega$. Since the variables x and y are separated in this equation, it can be used to construct low-rank approximations of the matrix G.

The GCA algorithm constructs an $\mathcal{H}^2$-matrix approximation [19, 8, 4] of G in four steps:

1. the index sets $\mathcal{I}$ and $\mathcal{J}$ are split hierarchically into *cluster trees*,
2. each cluster constructed in the first step is assigned a *cluster basis*,
3. the index set $\mathcal{I} \times \mathcal{J}$ is split hierarchically into a *block tree*, and finally
4. each block constructed in the third step is assigned either a *near-field matrix* or a *coupling matrix*.

The first three steps are adaptive, but require only a moderate fraction of the overall work. The fourth step is computationally expensive, but non-adaptive, so this step can be handled by GPGPUs.

A cluster tree $\mathcal{T}_\mathcal{I}$ for an index set $\mathcal{I}$ is a tree of subsets of $\mathcal{I}$. The root is the entire set $\mathcal{I}$ itself, and the sons $\operatorname{sons}(t)$ of a non-leaf node $t \in \mathcal{T}_\mathcal{I}$ correspond to a disjoint partition of their father. The nodes of a cluster tree are called *clusters*. Cluster trees can be constructed very efficiently by geometrically subdividing clusters [14].

A block tree $\mathcal{T}_{\mathcal{I}\times\mathcal{J}}$ for the index set $\mathcal{I} \times \mathcal{J}$ is a tree of subsets $t \times s$ of $\mathcal{I} \times \mathcal{J}$ with a *row cluster* $t \in \mathcal{T}_\mathcal{I}$ and a *column cluster* $s \in \mathcal{T}_\mathcal{J}$. The sons $\operatorname{sons}(t \times s)$ of a non-leaf node are the Cartesian products of the sons of t and the sons of s. The nodes of the block tree are called *blocks*. The block tree is used to identify submatrices that can be approximated by low rank: leaves are called *admissible* if they correspond to submatrices that can be approximated and *inadmissible* otherwise. Optimal block trees can be constructed using the cluster trees $\mathcal{T}_\mathcal{I}$ and $\mathcal{T}_\mathcal{J}$ and an *admissibility condition* that determines where an approximation scheme can be applied [14].

In the case of GCA, we rely on a geometric admissibility condition: clusters $t \in \mathcal{T}_\mathcal{I}$ and $s \in \mathcal{T}_\mathcal{J}$ are associated with axis-parallel *bounding boxes* $B_t, B_s \subseteq \mathbb{R}^3$ such that

$$\operatorname{supp} \varphi_i \subseteq B_t, \qquad \operatorname{supp} \psi_j \subseteq B_s \qquad \text{for all } i \in t,\ j \in s.$$

These bounding boxes can be constructed efficiently by merging bounding boxes for the individual triangles of the grid $\mathcal{G}$. Given an *admissibility parameter* $\eta \in \mathbb{R}_{>0}$, a pair $(t, s) \in \mathcal{T}_\mathcal{I} \times \mathcal{T}_\mathcal{J}$ of clusters is admissible, if

$$\max\{\operatorname{diam}(B_t), \operatorname{diam}(B_s)\} \leq \eta \operatorname{dist}(B_t, B_s)$$

holds.

Now we are in a position to apply (4). Given a cluster $t \in \mathcal{T}_\mathcal{I}$, we let $\delta_t := \operatorname{diam}(B_t)$ and construct an axis-parallel box $\omega_t \subseteq \mathbb{R}^3$ such that $B_t \subseteq \omega_t$ and

$$\operatorname{dist}(B_t, \partial\omega_t) = \delta_t/2.$$

It is easy to see that this property implies

$$\operatorname{dist}(B_s, \partial\omega_t) \geq \delta_t/2$$

for all admissible pairs $(t, s) \in \mathcal{T}_\mathcal{I} \times \mathcal{T}_\mathcal{J}$ (cf. [5, Lemma 3]), so the boundary $\partial\omega_t$ is sufficiently far from both B_t and B_s and we can apply (4) to approximate the kernel function.

For $i \in t$ and $j \in s$ we obtain

$$\begin{aligned} g_{ij} \approx \sum_{\nu=1}^{m} & \underbrace{\sqrt{w_\nu} \int_\Omega \varphi_i(x) g(x, z_\nu)\, dx}_{=:a_{t+,i\nu}} \\ & \times \underbrace{\sqrt{w_\nu} \int_\Omega \psi_j(y) \frac{\partial g}{\partial n(z_\nu)}(z_\nu, y)\, dy}_{=:b_{ts+,j\nu}} \\ - \sum_{\nu=1}^{m} & \underbrace{\sqrt{w_\nu}\delta_t \int_\Omega \varphi_i(x) \frac{\partial g}{\partial n(z_\nu)}(x, z_\nu)\, dx}_{=:a_{t-,i\nu}} \\ & \times \underbrace{\frac{\sqrt{w_\nu}}{\delta_t} \int_\Omega \psi_j(y) g(z_\nu, y)\, dy}_{=:b_{ts-,j\nu}} \end{aligned}$$

with the matrices $A_{t,+}, A_{t,-} \in \mathbb{C}^{t\times m}$ and $B_{t,+}, B_{t,-} \in \mathbb{C}^{s\times m}$ including suitable scaling factors. Introducing

$$A_t := \begin{pmatrix} A_{t,+} & A_{t,-} \end{pmatrix}, \qquad B_{ts} := \begin{pmatrix} B_{ts,+} & B_{ts,-} \end{pmatrix},$$

we can write our result in the short form

$$G|_{t\times s} \approx A_t B_{ts}. \tag{5}$$

It is important to note that the matrix A_t depends only on the row cluster t, but not on the column cluster s. This is a very attractive property, since the number of clusters is typically significantly smaller, frequently by a factor of 100 or more, than the number of blocks.

Experiments indicate that the rank $k = 2m$ of the approximation (5) is frequently far greater than necessary. In order to improve the efficiency, we apply the adaptive cross approximation algorithm [2] to the matrix A_t and obtain index sets $\tilde{t} \subseteq t$ and $\tau \subseteq \{1, \ldots, k\}$ such that

$$A_t \approx (A_t)_{t\times\tau} (A_t)^{-1}_{\tilde{t}\times\tau} (A_t)_{\tilde{t}\times k}. \tag{6}$$

The right-hand side of this equation can be interpreted as an "algebraic interpolation" by introducing

$$V_t := (A_t)_{t\times\tau} (A_t)^{-1}_{\tilde{t}\times\tau}$$

and the "restriction matrix" $R_t \in \mathbb{R}^{\tilde{t}\times t}$ satisfying

$$R_t u = u|_{\tilde{t}} \qquad \text{for all } u \in \mathbb{C}^t$$

such that $R_t A_t = A_t|_{\tilde{t}\times k}$, and writing (6) in the short form

$$A_t \approx \mathfrak{I}_t A_t \qquad \text{with} \qquad \mathfrak{I}_t := V_t R_t.$$

$\mathfrak{I}_t$ can be considered a Lagrange interpolation operator mapping from $\mathbb{C}^t$ into the range of A_t. The columns of V_t can be interpreted as Lagrange basis functions satisfying

$$R_t V_t = (A_t)_{\tilde{t}\times\tau} (A_t)^{-1}_{\tilde{t}\times\tau} = I,$$

and the restriction matrix as the pointwise evaluation of the interpolant.

Applying this interpolation operator to the submatrix $G|_{t\times s}$ and the approximation (5) yields

$$\mathfrak{I}_t G|_{t\times s} \approx \mathfrak{I}_t A_t B_{ts} \approx A_t B_{ts} \approx G|_{t\times s},$$

i.e., the interpolation error is under control, and

$$\mathfrak{I}_t G|_{t\times s} = V_t R_t G|_{t\times s} = V_t G|_{\tilde{t}\times s},$$

i.e., only the rows for the indices $\tilde{t} \subseteq t$ are required to construct the approximation.

2.4. $\mathcal{H}^2$-matrix

We can go one step further and apply the same arguments to the column cluster s instead of the row cluster t to obtain an index set $\tilde{s} \subseteq s$ and and interpolation operator $\mathfrak{I}_s = V_s R_s$ such that

$$G|_{t\times s} \mathfrak{I}_s^* \approx G|_{t\times s}, \qquad G|_{t\times s} \mathfrak{I}_s^* = G|_{t\times\tilde{s}} V_s^*,$$

and combining both interpolation operators yields

$$G|_{t\times s} \approx \mathfrak{I}_t G|_{t\times s} \mathfrak{I}_s^* = V_t G|_{\tilde{t}\times\tilde{s}} V_s^*.$$

The construction of the algebraic interpolation operators $\mathfrak{I}_t$ and $\mathfrak{I}_s$ is adaptive, but has to be performed only once per cluster. When these operators are available, the approximation for a block $t \times s$ can be constructed by evaluating the entries of $G|_{\tilde{t}\times\tilde{s}}$, i.e., by performing quadrature. We have already seen that GPGPUs are well-suited for this task, and only a very slight modification of our implementation is necessary.

We can improve the efficiency of the GCA scheme even further by constructing *nested* cluster bases: if $t \in \mathcal{T}_\mathcal{I}$ is a leaf, we proceed as before. Otherwise we first construct the interpolation operators for its sons. For the sake of simplicity, assume that there are two sons t_1, t_2 and that corresponding subsets $\tilde{t}_1 \subseteq t_1$, $\tilde{t}_2 \subseteq t_2$ and matrices V_{t_1}, V_{t_2} have already been

constructed. If $(t, s) \in \mathcal{T}_\mathcal{I} \times \mathcal{T}_\mathcal{J}$ is admissible, the same holds for (t_1, s) and (t_2, s), and we have

$$G|_{t\times s} = \begin{pmatrix} G|_{t_1\times s} \\ G|_{t_2\times s} \end{pmatrix} \approx \begin{pmatrix} V_{t_1} G|_{\tilde{t}_1\times s} \\ V_{t_2} G|_{\tilde{t}_2\times s} \end{pmatrix} = \begin{pmatrix} V_{t_1} & \\ & V_{t_2} \end{pmatrix} G|_{\hat{t}\times s}$$

with $\hat{t} := \tilde{t}_1 \cup \tilde{t}_2$. Applying cross approximation to the reduced matrix $\widehat{A}_t := A_t|_{\hat{t}\times k}$ instead of A_t yields a new interpolation operator with an index set $\tilde{t} \subseteq \hat{t}$ and a matrix $\widehat{V}_t$ such that

$$G|_{t\times s} \approx \begin{pmatrix} V_{t_1} & \\ & V_{t_2} \end{pmatrix} G|_{\hat{t}\times s} \approx \begin{pmatrix} V_{t_1} & \\ & V_{t_2} \end{pmatrix} \widehat{V}_t G|_{\tilde{t}\times s},$$

and we can define

$$V_t := \begin{pmatrix} V_{t_1} & \\ & V_{t_2} \end{pmatrix} \widehat{V}_t$$

to obtain the by now familiar form

$$G|_{t\times s} \approx V_t G|_{\tilde{t}\times s}.$$

Since $\hat{t}$ is typically a significantly smaller set than t, this recursive procedure can be significantly faster than the direct approach. The storage requirements are also reduced, since we have to store V_t only for leaf clusters and can use the smaller matrices $\widehat{V}_t$ for all other clusters. The resulting structure is known as an $\mathcal{H}^2$*-matrix* [19, 8, 4], the algebraic counterpart of fast multipole methods [26, 15], and it is possible to prove that the storage requirements and computational complexity of $\mathcal{H}^2$-matrices only grow linearly with the number of degrees of freedom and the rank. This makes them very attractive for large-scale computations.

3. Implementation

Although the previously mentioned computations are well-suited for GPGPUs in principle, we have to overcome a number of challenges in order to make the most of the available recources.

To set the stage, we consider a rough sketch of how a typical GPGPU works. It usually consists of n_{mp} *multiprocessors*, each equipped with n_{pe} arithmetic-logical *processing elements*. All processing elements of a given multiprocessor can either perform the same operation (addition, multiplication, comparison, jump, ...) or no operation in a given clock cycle. The SIMT (single instruction, multiple threads) programming model splits a computation into a number of *threads*, sequences of instructions that can be executed by the processing elements. Each thread is associated with an instruction counter that decides which instruction it has to execute next.

Since all processing elements of a multiprocessor have to perform the same operation in each cycle, the threads are bound together to form *warps*, each warp consisting of n_{pe} threads, and these warps are assigned to one of the multiprocessors.

In a clock cycle, each of the multiprocessors chooses a warp for execution, chooses an instruction, and performs the corresponding operation for all threads in the warp whose instruction counter matches the chosen instruction.

In order to take full advantage of all processing elements, it is therefore crucial that all threads, or at least all threads in each warp, execute the same instruction most of the time. Usually GPGPUs are "smart enough" to recover from threads that diverge only for a few cycles and then merge again, but it is our responsibility as programmers to keep these instances of instruction divergence as brief as possible.

Regarding our algorithm, the two most important problems are that

- near-field matrix blocks $G|_{t\times s}$ usually consist of a mix of all four cases of the Sauter-Schwab quadrature, each requiring a different number of quadrature points, and that
- a single block $G|_{t\times s}$ or $G|_{\tilde{t}\times\tilde{s}}$ is too small to take advantage of the thousands of processing elements provided by a modern GPGPU on its own.

The first issue is problematic since it means that mixing threads handling different cases within the same warp would lead to instruction divergence, the time for the execution of the warp would be (at best) determined by the longest-running thread.

The second issue poses a challenge since initiating the execution of a number of threads on a GPGPU typically requires a significant amount of bookkeeping on one hand and communication via a slow bus system on the other one. Some older GPGPUs even can only execute the same code on all multiprocessors, so running 10 threads on a GPGPU with 1 024 processing elements will lead to 1 014 processing elements doing nothing.

To address the first issue, we keep track of all integrals that appear in the course of the matrix assembly. Depending on the quadrature case, the indices of the triangles and the memory cell the integral belongs to in the matrix are be saved in individual lists for all four cases. If we launch threads on the GPGPU for all integrals in one of these lists, no instruction divergence can occur anymore, since all threads in one of the lists execute exactly the same instructions in exactly the same order.

A welcome side-effect of this approach is that we can control the size of these lists. This also addresses the second issue mentioned before: there is no longer a need for handing only a small number of integrals to the GPGPUS, we can choose the maximal size of the lists to strike a good balance between communication and bookkeeping overhead and ease of implementation. Experiments show that the size should be several megabytes to obtain a reasonable performance.

This algorithmic realization has some drawbacks as well: we have to allocate extra memory for the lists, but since the user can choose the size of the lists and since the storage can be re-used after one computation of a list has been finished, this is not a major drawback.

On the other hand, after the computations on the GPGPU have finished, the integrals have to be added to their final position in the stiffness matrix G. These memory operations have to be performed by the CPU, since we assume that only the CPU has a sufficient amount of memory at its disposal to store the matrix, and in a single-threaded program the GPGPU cannot do any further computations because the CPU is not able to

provide work to the GPGPU while copying data. Consequently, we propose to use multiple CPU threads to overcome this problem (cf. figure 3).

Of course, it would also be beneficial to let the CPU cores compute integrals, since they also contain SIMD units. Here we focus on an approach that has a single thread, in the following called the *master thread*, traverse the block tree and fill the lists with work items, while other CPU threads, called *worker threads* have the task to prepare the data in the lists for the GPGPU computation, launch appropriate threads on the GPGPU, and distribute the results back to the stiffness matrix. Essentially, we use a simple task scheduler following the producer-consumer pattern.

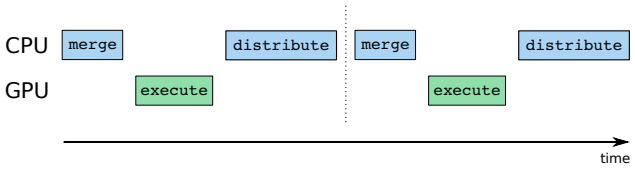
The implementation is based on the hierarchical matrix library *H2Lib*[2] written in the C programming language. For the realization of the task scheduler on the main processor, we employ OpenMP to create the master thread and a number of worker threads. The computations of the GPGPU are carried out using the OpenCL standard, which allows us to execute the quadrature code on any platform that implements OpenCL, not just on GPGPUs. Of course, our approach can also be applied with different threading libraries and different GPGPU APIs like CUDA.

In order to keep the amount of data that has to be communicated to the GPGPU small, we use a trick: in a first step, all integrals in a block $G|_{t\times s}$ are treated as if they were regular, i.e., as if they corresponded to disjoint triangles. This allows us to characterize the entire block just by the sets t and s, and we avoid having to send all indices of the Cartesian product $t \times s$ to the GPGPU. Of course, this will lead to wrong results if some of the integrals are singular, and so we recompute these problematic integrals in a second phase and fix the corresponding matrix entries. Although this means that some integrals will be computed "twice", the savings afforded by the reduction in communication more than make up for this overhead.

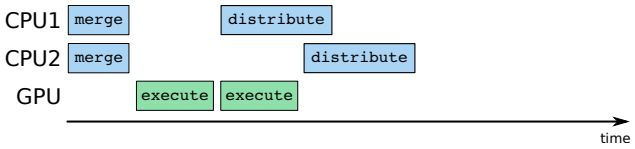
We split the assembly of the stiffness matrix into the following parts:

1. Set up all algebraic interpolation operators $\mathfrak{I}_t$ and $\mathfrak{I}_s$ for all subsets $t \subseteq \mathcal{I}$ and $s \subseteq \mathcal{J}$ on the CPU, since this cannot be properly vectorized.
2. Split the program execution into the execution of a master thread and several worker threads. The master thread traverses the block tree and adds each block to the list of regular integrals to be computed.
   As soon as the total size of one of these lists exceeds a given limit, the list is marked as "ready for execution" and handed over to the worker threads. This is depicted in algorithm 1.
3. Once a list has been marked as "ready for execution", a worker thread can fetch this list (cf. algorithm 2) and process this data package (see algorithm 3).
4. Once a work item has been processed on the GPGPU, the results need to be copied to their proper location in the stiffness matrix by the CPU. In case a block contains non-disjoint pairs of triangles, they are now added to the list for their respective case and handled as in (2) which is also displayed in algorithm 3.

[2]Available at `http://www.h2lib.org`



(a) GPGPU occupancy with a single worker thread



(b) GPGPU occupancy with two worker threads

Figure 1: Schematic difference of a single worker threads vs. two worker threads supplying a GPGPU with work items.

4. Numerical experiments

In this part we want to demonstrate the performance of our GPGPU algorithm for setting up boundary integral operators arising in the boundary element method.

For the following experiments we consider the solution of an interior Dirichlet problem for the Laplace equation in 3D. Let f be a harmonic function in a bounded domain $\Omega \subset \mathbb{R}^3$ and assume that the Dirichlet values $f|_{\partial\Omega}$ are given. In the context of the boundary element method, this translates to the boundary integral equation

$$\int_{\partial\Omega} g(x,y)\frac{\partial f}{\partial n}(y)\,dy = \frac{1}{2}f(x) + \int_{\partial\Omega}\frac{\partial g}{\partial n(y)}(x,y)f(y)\,dy \qquad (7)$$

for (almost) all $x \in \partial\Omega$. We are looking for the Neumann values $\frac{\partial f}{\partial n}$. Here the kernel function

$$g(x,y) := \frac{1}{4\pi\|x-y\|}$$

is the fundamental solution of the Laplace operator in 3D.

A Galerkin discretization of this equation with piece-wise constant basis functions $(\varphi_i)_{i\in\mathcal{I}}, (\psi_j)_{j\in\mathcal{J}}$ leads to a linear system

$$V\alpha = \left(\frac{1}{2}I + K\right)\beta,$$

where the coefficients of the matrices V and K are given by equation (1) with the kernel functions g and $\frac{\partial g}{\partial n(y)}$, respectively. The values of f and $\frac{\partial f}{\partial n}$ are represented in the bases as $f = \sum_{j\in\mathcal{J}}\beta_j\psi_j$ and $\frac{\partial f}{\partial n} = \sum_{i\in\mathcal{I}}\alpha_i\varphi_i$, respectively. Since the matrix V is symmetric and positive definite, we can employ a conjugate gradient method [22] to solve the linear system.

Algorithm 1 Assembly of a boundary integral operator G. The parameters of all near-field and far-field blocks are initially added to the list of disjoint triangles. The procedure ADD_BLOCK takes care that these lists do not become too big and are queued for execution by the scheduling algorithm once they reach a given size.

```
procedure ADD_BLOCK(b)
    if SIZEOF(ℓ) + SIZEOF(b) < maxsize then
        ADD_TO_LIST(ℓ,b)
    else
        ENQUEUE_LIST(ℓ)
        ℓ = NEW_LIST(maxsize)
        if SIZEOF(ℓ) + SIZEOF(b) < maxsize then
            ADD_TO_LIST(ℓ,b)
        else
            (b1,b2) ← SPLIT_BLOCK(b)
            ADD_BLOCK(b1)
            ADD_BLOCK(b2)
        end if
    end if
end procedure

procedure ASSEMBLE_GPU(G)
    for all matrix blocks b ∈ {G_{|t×s}, G_{|t̂×ŝ}} do
        ADD_BLOCK(b)
    end for
end procedure
```

Algorithm 2 Basic sketch of the scheduler algorithm that is used. As long as new lists are available, each thread fetches a list and either executes it on the CPU or on the GPGPU depending on its affinity. When running out of lists to be processed, a thread goes to sleep for a short period of time or terminates if no more lists are to be expected.

```
procedure SCHEDULE_TASKS
    while ℓ ← DEQUEUE_LIST do
        if ℓ ≠ empty then
            if AFFINITY(ℓ) = GPU then
                EXECUTE_GPU(ℓ)
            else
                EXECUTE_CPU(ℓ)
            end if
        else
            SLEEP
        end if
    end while
end procedure
```

Algorithm 3 Accumulation for regular integrals. If a block also contains non-disjoint pairs of triangles, corresponding to singular integrals, they are now added to the list of their respective case and processed in a similar way.

```
procedure DISTRIBUTE_RESULTS_DISJOINT(ℓ, data)
    for all G_{|t×s} ∈ ℓ do
        COPY_RESULTS(data, G_{|t×s})
        if G_{|t×s} contains non-disjoint pairs of triangles then
            for all (i, j) ∈ G_{|t×s} do
                v ← NUMBER_OF_COMMON_VERTICES(t, s)
                if v > 0 then
                    ADD_ENTRY_TO_LIST(ℓ_v, (i, j))
                end if
            end for
        end if
    end for
end procedure
```

Algorithm 4 Executing a list ℓ on the GPGPU. The parameters of the individual integrals have to be copied into contiguous chunks of memory to be transferred to the GPGPU before the threads can be launched on the GPGPU. After completion, the results have to be copied back to main memory and distributed in the matrix G.

```
procedure EXECUTE_GPU(ℓ)
    data ← MERGE_DATA(ℓ)
    INVOKE_GPU_KERNEL(data)
    DISTRIBUTE_RESULTS(ℓ, data)
    CLEANUP(data)
end procedure
```

The most time-consuming part of the whole computation is the setup of the matrices V and K, which is carried out mostly by the GPGPU. Due to the symmetry of V, we only have to compute its lower triangular part. The setup times for K are roughly twice those for the matrix V, not only due to the fact that the entire matrix K is constructed, but also since the kernel function of K requires more operations than the one for V.

In order to verify the correctness of our proposed method, we solve the system with the following three harmonic functions:

$$f_1(x) = x_1^2 - x_3^2, \qquad f_2(x) = g(x, (1.2, 1.2, 1.2)),$$
$$f_3(x) = g(x, (1.0, 0.25, 1.0)).$$

As a simple test domain we use the unit sphere

$$\Omega_s = \{x \in \mathbb{R}^3 \ : \ \|x\|_2 = 1\},$$

approximated by a triangulation constructed by regularly subdividing the eight triangles forming the double pyramid $\Omega_p = \{x \in \mathbb{R}^3 \ : \ \|x\|_1 = 1\}$ into subtriangles and projecting the vertices to Ω_s.

CPU algorithm. To have a reference point for our further experiments, we first present some results computed entirely on the CPU. Instead of traversing the block tree and keeping account of the the arising matrix sub-blocks to be computed, the CPU algorithm directly computes these matrix entries. The algorithm was executed on a Intel Core i7-3820 processor with 4 cores and hyper-threading enabled, which allows us to use up to 8 threads on the CPU. Consequently, we want to use all 8 threads to execute the algorithm on the CPU in order to keep pace with the GPGPUs later on. The quadrature routines employ vectorization based on AVX. The results can be seen in Figure 2. The timings do not include the setup time for the algebraic interpolation operators, since these are always precomputed by a CPU algorithm. In this and all later experiments we scale the runtime by the number of degrees of freedom in order to compare the values across a wide range of resolutions of the geometry. We can see in Figure 2 that the runtime on the main processor is between 150 and 650 microseconds (μs) for both the SLP operator V and the DLP operator K for all resolutions.

The increase in time per degree of freedom is due to higher accuracies for the GCA algorithm: as we refine the grid, the condition number of V grows, and we have to approximate the matrix more accurately in order to preserve the convergence rate of the original (uncompressed) boundary element method. The parameters of the GCA approximation scheme are chosen as in [5] to ensure $O(h)$ convergence of the Neumann values and to keep them close to the discretization error. The increase in accuracy leads to the poly-logarithmic growth observed in Figure 2.

List size. Now we consider the performance of our GPGPU algorithm, starting with the influence of the size of lists that are collected before being sent to the GPGPUs. It seems obvious

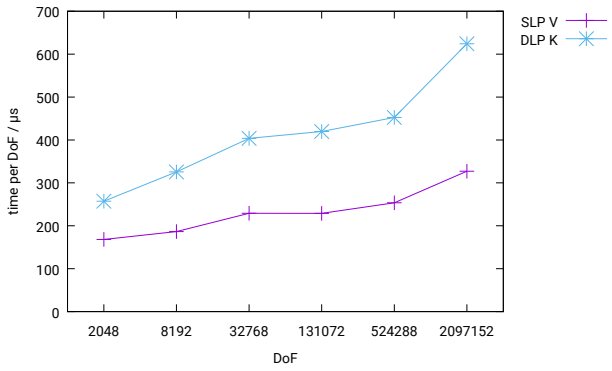


Figure 2: Setup time of the boundary integral operators on different resolutions of the unit sphere. Only CPU threads are employed to calculate the integrals.

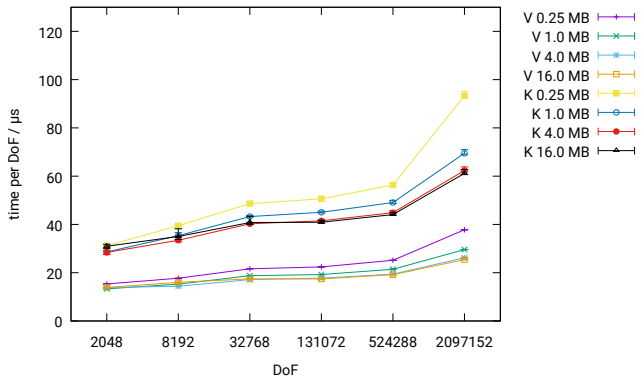
that a smaller size automatically corresponds to more interactions between CPU and GPGPUS, and since each transfer between CPU and GPGPU involves some overhead, it is not surprising that smaller list sizes lead to longer execution times of our algorithm. The setup times for different list sizes and different resolutions are given in Figure 3.

Due to the non-deterministic behaviour of the schedulers both on the CPU and the GPGPU, we have run the computations five times on the GPGPU and noted the minimal, maximal, and average runtimes of the algorithm. These are depicted by the error-bars in Figure 3 and the following ones. We can see that the deviation is larger for very small list sizes and negligible for larger ones. The main conclusion drawn from figure 3 is that the list size should be chosen somewhere around 4–16 MB to minimize the runtime. However this is not the best choice in all cases. In general there is no best choice for all degrees of freedom for this parameter, but 8 MB seems to be a good empirical value.

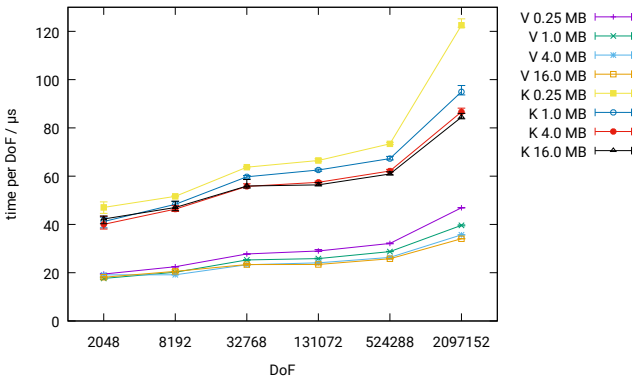
Remark 1. *At the first glance, the results from figure 3 appear surprising because the GeForce GTX 680 card achieves a lower performance than its architectural predecessor, the GeForce GTX 580. But in fact, this can be explained by changes in the GPGPU's internal structure, especially for double precision computations. The theoretical peak performance of the GeForce GTX 680 is given by 128.8 GFlops and the peak performance of the GeForce GTX 580 is given as 197.6 GFlops in double precision. Therefore we can expect the GeForce GTX 580 to be faster than the GeForce GTX 680 by a factor of 1.5 which is confirmed by our results.*

In comparison, the current GeForce GTX 1080 card is reported to reach 277 GFlops in double precision computations, so we expect it to be only about 50% faster than the GTX 580.

Worker threads. Since there is always a portion of time in between two successive kernel calls on the GPGPU where the CPU has to perform some data management operations, the utilization of the GPGPU will not be near its maximum. Therefore our implementation of the algorithm has a parameter controlling the number of CPU worker threads spawned per GPGPU to supply the GPGPU with work. We now investigate the effect



(a) Runtime for V and K on GeForce GTX 580



(b) Runtime for V and K on GeForce GTX 680

Figure 3: Setup time of the boundary integral operators for varying list sizes on different resolutions of the unit sphere. An NVIDIA GeForce GTX 580 was used to compute the SLP operator V and the DLP operator K in 3(a). Likewise an NVIDIA GeForce GTX 680 was used to compute the SLP and DLP operators in 3(b).

of the number of worker threads on the overall performance of our approach.

In Figure 4 we can see a significant reduction of the runtime when two or more worker threads are employed per GPGPU. It is not necessary to use more than two threads per GPGPU. Indeed using more than two threads might have a negative impact on the performance if not enough hardware threads are available to supply the GPGPUs with sufficient work or the memory bandwidth of the CPU might be exhausted at some point. We can also observe that the deviation in runtime increases for smaller resolutions of the geometry and decreases for bigger resolutions as more worker threads are employed. This might be due to the non-deterministic behaviour of CPU thread scheduling by the operating system. Additionally, for very small numbers of unknowns using more worker threads can also influence the runtime in a negative way because there is not enough work to distribute and some threads might be idle.

Multi-GPU setup. In the design of our algorithm, we took into account that a system can have more than just one GPGPU available. A single worker thread is always directly connected with a single GPGPU and cannot supply work to a different GPGPU. With this concept it is very straightforward to employ all GPGPUs in a system to work on the same problem. On the other hand, all GPGPUs are connected by the same PCIe bus system in typical computer systems, and it is not quite clear if the total amount of data that is being transferred over this bus can be handled without any delay. We investigate this behaviour in the next experiment, where we employ both a GeForce GTX 580 and GeForce GTX 680 at the same time. In this context we are interested in how the runtime of our algorithm scales when using both cards simultaneously. Figure 5 illustrates the effect of the multi-GPU setup.

At least for this two-GPU setup, our approach appears to scale well. According to our previous remark about the peak performances of both GPGPUs we can only expect the runtime for the two-GPU setup of our algorithm to be smaller by a factor of 1.7 compared to the runtime of the GeForce GTX 580 or smaller by a factor of 2.5 compared to the runtime of the GeForce GTX 680. Indeed our experiments show similar factors, and we can say that our scheduler handles the two-GPU setup quite well.

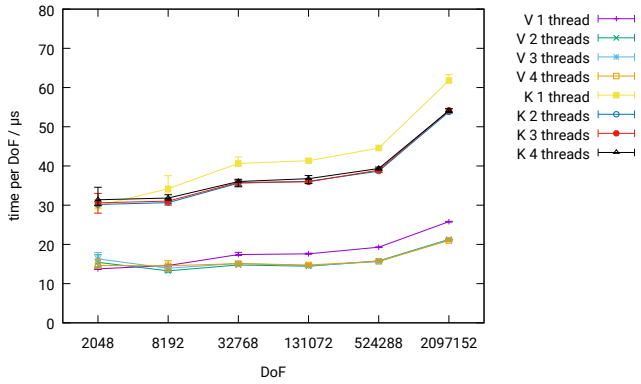
The scaling behaviour of our algorithm on more than two GPGPUs is an interesting topic and will be part of future research.

Tables 1 and 2 list the absolute computing times for our algorithm and also include the setup time for the algebraic interpolation operators for the sake of completeness, although they are computed entirely on the CPU. We observe that the time required to set up the interpolation operators is roughly the same as the time required by the setup of the near-field and coupling matrices on both GPGPUs.

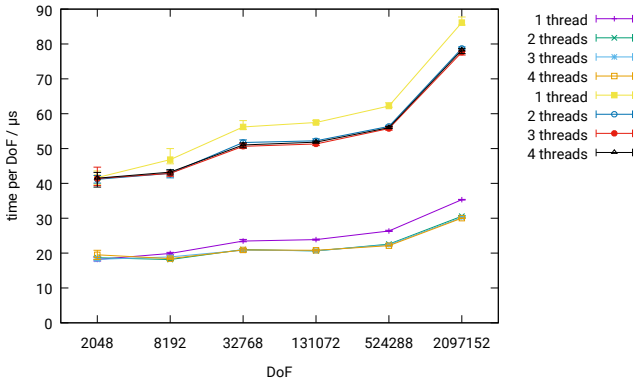
We could speed up computation of the interpolation operators as well, either by using SIMD instructions and multiple cores on the CPU or with the help of GPGPUs.

More important is the time needed to solve the three linear systems. We used a simple conjugate gradient method which needed 260 steps on the finest mesh and took about 1400 seconds for each right-hand side. At this point a good preconditioner would be very desirable. The *H2Lib* package offers $\mathcal{H}^2$-Cholesky and $\mathcal{H}^2$-LU decompositions, but unfortunately these are not yet parallelized. Hence a comparison with a sequential algorithm for constructing a preconditioner would not be fair.

Higher quadrature orders. All experiments so far have been conducted with a basic one dimensional Gaussian quadrature formula with 3 points for Duffy transformations and with 5 points for the Sauter-Schwab quadrature formulas. In some applications this quadrature order might not be sufficient if the geometries become less smooth. Therefore we also present some results for a basic Gaussian quadrature formula with 4(6) quadrature points in Table 3. Since the unit sphere is a very smooth geometry, such a high quadrature order is not really necessary, but we can see that the GPGPUs benefit from the higher order, since their efficiency increases with the amount of work required for a single integral. Hence the speedup factor

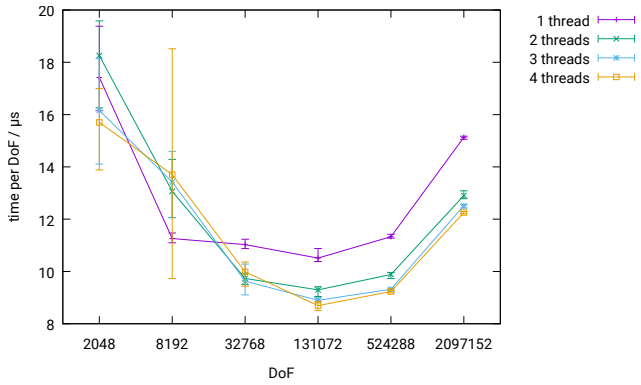


(a) Runtime for V and K on GeForce GTX 580

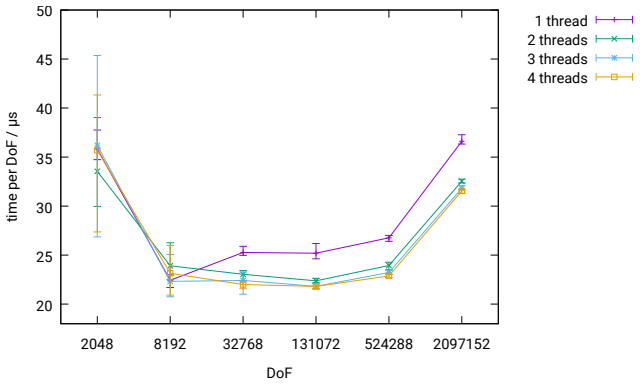


(b) Runtime for V and K on GeForce GTX 680

Figure 4: Setup time of the boundary integral operators for varying number of worker threads per GPGPU on different resolutions of the unit sphere. The list size was chosen constant as 8 MB. An NVIDIA GeForce GTX 580 was used to compute the SLP matrix V and the DLP matrix K in 4(a). Likewise an NVIDIA GeForce GTX 680 was used to compute the SLP and DLP matrices in 4(b).



(a) Runtime for V on GeForce GTX 580 and 680



(b) Runtime for K on GeForce GTX 580 and 680

Figure 5: Setup time of the boundary integral operators using both GeForce GTX 580 and GeForce GTX 680 to compute the integrals. The list size is kept constant at 8 MB and two worker threads are being employed per GPGPU.

Table 1: Runtimes for CPU and GPGPU algorithms to setup SLP operator V. List size is kept constant at 8 MB and 2 worker threads are employed.

DoFs	$\Im_t, \Im_s$	CPU	GTX 580	GTX 680	GTX 580 + 680
2048	<0.1 s	0.3 s	<0.1 s	<0.1 s	<0.1 s
8192	0.1 s	1.5 s	0.1 s	0.2 s	0.1 s
32768	0.4 s	7.5 s	0.5 s	0.7 s	0.3 s
131072	1.5 s	30.0 s	1.9 s	2.7 s	1.2 s
524288	6.2 s	133.0 s	8.3 s	11.8 s	5.2 s
2097152	62.0 s	686.2 s	44.6 s	64.1 s	27.1 s

Table 2: Runtimes for CPU and GPGPU algorithms to setup DLP operator K. List size is kept constant at 8 MB and 2 worker threads are employed.

DoFs	$\Im_t, \Im_s$	CPU	GTX 580	GTX 680	GTX 580 + 680
2048	<0.1 s	0.5 s	<0.1 s	<0.1 s	<0.1 s
8192	0.1 s	2.7 s	0.3 s	0.4 s	0.2 s
32768	0.5 s	13.2 s	1.2 s	1.7 s	0.8 s
131072	1.7 s	55.0 s	4.7 s	6.8 s	2.9 s
524288	6.7 s	237.3 s	20.3 s	29.5 s	12.5 s
2097152	70.2 s	1309.0 s	112.8 s	165.1 s	68.2 s

compared to the CPU implementation rises from 25.3 to 29.8 for the single layer potential and from 19.2 to 22.3 for the double layer potential.

Helmholtz equation. As a final example we consider a slightly different problem setting: the Helmholtz equation in its BEM formulation. In this case we would like to solve the exterior Dirichlet problem, given by

$$\begin{aligned} \Delta u(x) + \kappa^2 u(x) &= 0, & x &\in \mathbb{R}^3 \setminus \bar{\Omega} \\ u(x) &= f(x), & x &\in \partial\Omega, \\ \left\| \left\langle \nabla u(x), \frac{x}{\|x\|} \right\rangle - \iota\kappa u(x) \right\| &\in O\left(\frac{1}{\|x\|^2}\right) & \|x\| &\to \infty. \end{aligned}$$

Here $\kappa \in \mathbb{R}_{>0}$ denotes the wave number. It is well known that if κ is close to an eigenvalue of the interior Neumann problem, the standard Dirichlet-to-Neumann mapping (7) is not applicable due to the single layer potential operator not being coercive anymore. Well-known proposals to fix this problem are the Brakhage-Werner approach [10] and the Burton-Miller approach [11]. We choose the former and reformulate the problem as

$$\int_{\partial\Omega} \frac{\partial g}{\partial n(y)}(x,y) w(y) \mathrm{d}y - \iota\eta \int_{\partial\Omega} g(x,y) w(y) \mathrm{d}y = f(x)$$

for all $x \in \mathbb{R}^3 \setminus \bar{\Omega}$, which has to be solved for the unknown density w. To ensure unique solvability, we have to choose $\eta > 0$. Applying trace operators yields a boundary integral equation which we can solve with the same techniques as (7).

Again we define single and double layer potential operators V and K using the fundamental solution

$$g(x,y) := \frac{\exp(\iota\kappa\|x-y\|}{4\pi\|x-y\|}$$

of the Helmholtz equation. Now we want to demonstrate the computing power of the two GPGPUs combined against all four CPU cores. In the same way as we did for Laplace's equation, we have chosen the geometry to be the unit sphere and computed the solution up to discretization error for different resolutions of the sphere, but with a constant wave-number $\kappa = 3$. As Dirichlet data we choose the function

$$f(x) = g(x, (0.0, 0.0, 0.2)).$$

Since we do not have an analytic solution for w at our disposal, we evaluate the solution u of the Helmholtz equation by the Brakhage-Werner formulation and compare it to the analytical solution of the problem in the exterior of the domain, given by the function f itself. The results can be seen in Table 4.

5. Conclusions

Matrices arising from the Galerkin discretization of boundary integral equations are densely populated and therefore very compute-intensive. We have proposed an implementation of the Green cross approximation algorithm on GPGPUs and have shown that this approach is very fast compared to pure CPU code, allowing us to set up very large problems quickly.

We have also shown that both the GCA method and our implementation on the GPGPU work not only for the Laplace equation, but also for the significantly more challenging Helmholtz equation.

Our implementation is not limited to graphics cards, but can utilize general computing hardware as long as it supports the OpenCL standard. The option to use of more that just one accelerator card makes this approach very interesting for high performance computing applications because it might be scaled to several hundreds of GPGPUs with some modifications.

Until now, the setup phase of the boundary integral matrices has dominated the computing time of boundary element methods. Using our new CPU/GPGPU approach, the time required for solving the linear system has become the limiting factor. This challenge could be approached, e.g., by parallelizing $\mathcal{H}$- and $\mathcal{H}^2$-matrix preconditioners [14, 9, 23].

References

[1] C. R. Anderson. An implementation of the fast multipole method without multipoles. *SIAM J. Sci. Stat. Comp.*, 13:923–947, 1992.

[2] M. Bebendorf and S. Rjasanow. Adaptive Low-Rank Approximation of Collocation Matrices. *Computing*, 70(1):1–24, 2003.

[3] M. Bebendorf and R. Venn. Constructing nested bases approximations from the entries of non-local operators. *Num. Math.*, 121(4):609–635, 2012.

[4] S. Börm. *Efficient Numerical Methods for Non-local Operators: $\mathcal{H}^2$-Matrix Compression, Algorithms and Analysis*, volume 14 of *EMS Tracts in Mathematics*. EMS, Zürich, 2010.

[5] S. Börm and S. Christophersen. Approximation of integral operators by Green quadrature and nested cross approximation. *Num. Math.*, 133(3):409–442, 2016.

[6] S. Börm and J. Gördes. Low-rank approximation of integral operators by using the Green formula and quadrature. *Numerical Algorithms*, 64(3):567–592, 2013.

[7] S. Börm and L. Grasedyck. Hybrid cross approximation of integral operators. *Numer. Math.*, 101:221–249, 2005.

[8] S. Börm and W. Hackbusch. Data-sparse approximation by adaptive $\mathcal{H}^2$-matrices. *Computing*, 69:1–35, 2002.

[9] S. Börm and K. Reimer. Efficient arithmetic operations for rank-structured matrices based on hierarchical low-rank updates. *Comp. Vis. Sci.*, 16(6):247–258, 2015. `http://arxiv.org/abs/1402.5056`.

[10] H. Brakhage and P. Werner. Über das dirichletsche Außenraumproblem für die helmholtzsche schwingungsgleichung. *Archiv der Mathematik*, 16(1):325–329, 1965.

[11] A. J. Burton and G. F. Miller. The application of integral equation methods to the numerical solution of some exterior boundary-value problems. *Proceedings of the Royal Society of London. Series A, Mathematical and Physical Sciences*, 323(1553):pp. 201–210, 1971.

[12] S. Erichsen and S. A. Sauter. Efficient automatic quadrature in 3-d Galerkin BEM. *Comput. Meth. Appl. Mech. Eng.*, 157:215–224, 1998.

[13] Z. Gimbutas and V. Rokhlin. A generalized fast multipole method for nonoscillatory kernels. *SIAM J. Sci. Comput.*, 24(3):796–817, 2002.

[14] L. Grasedyck and W. Hackbusch. Construction and arithmetics of $\mathcal{H}$-matrices. *Computing*, 70:295–334, 2003.

[15] L. Greengard and V. Rokhlin. A fast algorithm for particle simulations. *J. Comp. Phys.*, 73:325–348, 1987.

[16] L. Greengard and V. Rokhlin. A new version of the fast multipole method for the Laplace equation in three dimensions. In *Acta Numerica 1997*, pages 229–269. Cambridge University Press, 1997.

[17] W. Hackbusch. A sparse matrix arithmetic based on $\mathcal{H}$-matrices. Part I: Introduction to $\mathcal{H}$-matrices. *Computing*, 62:89–108, 1999.

Table 3: Runtimes for CPU and GPGPU algorithms to setup SLP V and DLP operator K for basic quadrature rules using 4(6) points. List size is kept constant at 8 MB and 2 worker threads are employed. For the last line, the GCA parameter $\delta = 2$ was chosen instead of $\delta = 1$ to make the problem fit into memory.

DoFs	CPU SLP	GTX 580 + 680 SLP	CPU DLP	GTX 580 + 680 DLP
2048	1.0 s	<0.1 s	1.5 s	0.1 s
8192	4.8 s	0.2 s	7.7 s	0.4 s
32768	21.6 s	0.7 s	39.0 s	1.8 s
131072	86.8 s	2.8 s	162.1 s	7.3 s
524288	368.5 s	12.0 s	702.0 s	31.3 s
2097152	1439.3 s	48.3 s	2936.2 s	131.9 s

Table 4: Runtimes for quad-core CPU and GPGPU algorithms to setup the SLP matrix V the and DLP matrix K for the Helmholtz equation. List size is kept constant at 8 MB and 2 worker threads are employed for the GPGPUs.

DoFs	CPU SLP	GTX 580 + 680 SLP	CPU DLP	GTX 580 + 680 DLP
2048	2.3 s	0.1 s	2.7 s	0.1 s
8192	9.6 s	0.3 s	11.8 s	0.4 s
32768	42.7 s	1.3 s	55.2 s	1.8 s
131072	205.8 s	6.7 s	263.4 s	8.9 s
524288	843.6 s	27.9 s	1050.1 s	36.9 s

[18] W. Hackbusch and B. N. Khoromskij. A sparse matrix arithmetic based on $\mathcal{H}$-matrices. Part II: Application to multi-dimensional problems. *Computing*, 64:21–47, 2000.

[19] W. Hackbusch, B. N. Khoromskij, and S. A. Sauter. On $\mathcal{H}^2$-matrices. In H. Bungartz, R. Hoppe, and C. Zenger, editors, *Lectures on Applied Mathematics*, pages 9–29, Berlin, 2000. Springer-Verlag.

[20] W. Hackbusch and Z. P. Nowak. On the fast matrix multiplication in the boundary element method by panel clustering. *Numer. Math.*, 54:463–491, 1989.

[21] S. Hamada. Performance comparison of three types of GPU-accelerated indirect boundary element method for voxel model analysis. *International Journal of Numerical Modelling: Electronic Networks, Devices and Fields*, 26(4):337–354, 2013.

[22] M. R. Hestenes and E. Stiefel. Methods of conjugate gradients for solving linear systems. *J. Res. Nat. B. Stand.*, 49(6), 1952.

[23] R. Kriemann. $\mathcal{H}$-LU factorization on many-core systems. *Comp. Vis. Sci.*, 16(3):105–117, 2013.

[24] J. Labaki, L. O. S. Ferreira, and E. Mesquita. Constant boundary elements on graphics hardware: a GPU-CPU complementary implementation. *Journal of the Brazilian Society of Mechanical Sciences and Engineering*, 33:475 – 482, 12 2011.

[25] G. Of, O. Steinbach, and W. L. Wendland. The fast multipole method for the symmetric boundary integral formulation. *IMA J. Numer. Anal.*, 26:272–296, 2006.

[26] V. Rokhlin. Rapid solution of integral equations of classical potential theory. *J. Comp. Phys.*, 60:187–207, 1985.

[27] S. A. Sauter. *Über die effiziente Verwendung des Galerkin-Verfahrens zur Lösung Fredholmscher Integralgleichungen*. Doctoral thesis, Christian-Albrechts-Universität Kiel, 1992.

[28] S. A. Sauter. Variable order panel clustering (extended version). Preprint 52/1999, Max-Planck-Institut für Mathematik, Leipzig, Germany, 1999.

[29] S. A. Sauter and C. Schwab. *Boundary Element Methods*. Springer, Berlin, Heidelberg, 2011.

[30] C. Schwab and W. L. Wendland. Numerical evaluation of singular and finite-part integrals on curved surfaces using symbolic manipulation. *Computing*, 49(3):279–301, 1992.

[31] T. Takahashi and T. Hamada. GPU-accelerated boundary element method for Helmholtz' equation in three dimensions. *International Journal for Numerical Methods in Engineering*, 80(10):1295–1321, 2009.

[32] Y. Wang, Q. Wang, X. Deng, Z. Xia, J. Yan, and H. Xu. Graphics processing unit (GPU) accelerated fast multipole BEM with level-skip M2L for 3D elasticity problems. *Advances in Engineering Software*, 82:105 – 118, 2015.

[33] L. Ying, G. Biros, and D. Zorin. A kernel-independent adaptive fast multipole algorithm in two and three dimensions. *J. Comp. Phys.*, 196(2):591–626, 2004.